LAWRENCE
LIVERMORE
NATIONAL
LABORATORY

LLNL-JRNL-403480

High resolution 17 keV to 75 keV backlighters for High Energy Density experiments

H.-S. Park, B. R. Maddox, E. Giraldez, S. P. Hatchett, L. Hudson, N. Izumi, M. H. Key, S. Le Pape, A. J. MacKinnon, A. G. MacPhee, P. K. Patel, T. W. Phillips, B. A. Remington, J. F. Seely, R. Tommasini, R. Town, J. Workman

May 5, 2008

Physics of Plasmas Journal

Disclaimer

High resolution 17 keV to 75 keV backlighters for High energy density experiments

H.-S. Park[1], B. R. Maddox[1], E. Giraldez[2], S. P. Hatchett[1], L. T. Hudson[3], N. Izumi[1], M. H. Key[1], S. Le Pape[1], A. J. MacKinnon[1], A.G. MacPhee[1], P. K. Patel[1], T. W. Phillips[1], B. A. Remington[1], J. F. Seely[4], R. Tommasini[1], R. Town[1], J. Workman[5]

[1] *Lawrence Livermore National Laboratory, Livermore, CA 94550, USA*

[2] *General Atomics, San Diego,CA 92121, USA*

[3] *NIST, Gaithersburg, MD 20899 USA*

[4] *Naval Research Laboratory, Washington, DC 20375, USA*

[5] *Los Alamos National Laboratory, Los Alamos, NM 87545, USA*

Abstract

We have developed 17 keV to 75 keV 1-dimensional and 2-dimensional high-resolution (< 10 μm) radiography using high-intensity short pulse lasers. High energy K-α sources are created by fluorescence from hot electrons interacting in the target material after irradiation by lasers with intensity $I_L > 10^{17}$ W/cm^2. We have achieved high resolution point projection 1-dimensional and 2-dimensional radiography using micro-foil and micro-wire targets attached to low-Z substrate materials. The micro-wire size was 10 μm x 10 μm x 300 μm on a 300 μm x 300 μm x 5 μm CH substrate. The radiography performance was demonstrated using the Titan laser at LLNL. We observed that the resolution is dominated by the micro-wire target size and there is very little degradation from the plasma plume, implying that the high energy x-ray photons are generated mostly within the micro-wire volume. We also observe that there are enough Kα

photons created with a 300 J, 1-ω, 40 ps pulse laser from these small volume targets, and that the signal-to-noise ratio is sufficiently high, for single shot radiography experiments. This unique technique will be used on future high energy density (HED) experiments at the new Omega-EP, ZR and NIF facilities.

I. INTRODUCTION

Laser driven x-ray sources are used in many applications. Considerable progress has been made in medical imaging where K-α sources from the ultra short pulses are used for angiography[1] and phase-contrast imaging[2]. These experiments radiograph mostly low-Z targets and very often use multiple pulses to accumulate enough photons to acquire adequate signal levels. For ICF and HED experiments where most of experiments are single event the backlighters have to provide enough photons for one shot. Conventional laser-based radiography has traditionally used x-ray emission from thermal plasma sources with moderately high efficiencies. While these sources have been sufficient for previous experiments a wide range of high energy density (HED) experiments on new laser facilities such as the Omega-Enhanced performance (EP)[3], the Z Refurbished (ZR)[4], and the National Ignition Facility (NIF)[5] will require backlighters that can probe high areal density materials with high resolution. For these proposed experiments, efficient higher-energy x-ray sources are required. It has been shown that a significant decrease in efficiency of traditional thermal sources leads to a limiting x-ray energy near 10-keV. Short pulse non-thermal laser interactions with solid target materials have been demonstrated to produce sufficient x-ray generation above 10-keV for radiography of dense targets. Example experiments that require high-energy x-ray radiography include the study of

material properties (such as material strength) at very high pressure[6] and mid- to high-Z capsule implosion experiments[7] as depicted in Fig 1. In a material strength experiment, a sinusoidally-rippled sample material is compressed at high pressure and accelerated by a laser plasma-piston drive[8], such that the rippled surface is hydrodynamically unstable. The ripples grow in amplitude due to the Rayleigh-Taylor (RT) instability, and the material strength retards this growth[9]. The growth rate can be measured by in-flight radiography, and material strength inferred by comparison with 2D hydrodynamic simulations including a model for high-pressure material strength. In this experiment, the backlighter x-ray energy is dictated by the sample material types and their thicknesses. For aluminum or vanadium samples of ~35 μm thickness, 4.3 keV or 5.2 keV thermal He-α backlighters are sufficient to obtain high contrast radiographs of RT growth factors of ~10. On NIF, we plan to study Ta or other high-Z materials of ~100 μm thickness. In this case, we will need backlighter x-ray energies of > 40 keV. The second example is radiography of imploding capsules that are made of mid- to high-Z materials. Unlike CH or Be ignition capsules, these mid-Z capsules will have high areal core densities when they are compressed. Again, we will need > 40 keV backlighters to image spatial features on these targets which cannot be obtained from traditional thermal x-ray sources.

The K-α emission mechanism using high intensity lasers is a promising way of creating 20 keV to 100 keV high energy x-rays. When a laser with intensity > 10^{17} W/cm^2 strikes a target, a forward directed "spray" of energetic electrons is created, with energies as high as ~100 MeV[10]. This forward current draws a return current, and a very strong azimuthal magnetic field is created, with a strength predicted to be 10 MG to 100 MG or higher. The target also becomes charged, causing all but the most energetic electrons to return for multiple passes through the target ("refluxing"). As these energetic electrons traverse the target, bound electrons can be

knocked out by electron-electron scattering. If a K-shell electron is knocked out, this inner shell vacancy is quickly filled by an L-shell or M-shell electron, generating isotropic K–α or K-β radiation.

We have demonstrated that the high energy x-rays generated by high intensity lasers are created within the high-density bulk part of the target material. High resolution 1-dimensional radiography can therefore be achieved by irradiating a thin micro-foil viewed edge-on[11]. As illustrated in Fig 2, the spatial resolution for this edge-on 1-dimensional radiography technique is determined by the micro-foil thickness, since the x-ray source generation is confined to the high-density region of the micro-foil. Our previous work demonstrated radiography using a 40 keV samarium backlighter that achieved 10 μm spatial resolution. This radiography technique is applied to an integrated experiment that measured the absolute equation of state of aluminum under shock driven condition[12]. In this paper, we present an extension of our 1-dimensional radiography work to higher energies of 68 keV, and to 2-D using micro-wires viewed edge-on, as shown in Fig 2b

II. EXPERIMENTAL SET-UP

We performed several experiments at the Titan Laser to demonstrate high-energy radiography. Titan uses chirped-pulse amplification[13], or CPA, to generate short-pulse (1ps to 50 ps), high-power (100 TW) beams. In this CPA system a short (10 fs to 200 fs), low energy (~ 1 nJ) pulse is generated by a mode-locked oscillator in the front end. This short pulse is stretched in time to ~3 ns then amplified to the 10 J to 300 J level. In the final stage of CPA, the amplified, chirped pulse is temporally compressed back to its original duration. This re-compressed pulse is

then focused via an off-axis f/3 parabola creating a small laser spot. The small spot size and the short pulse duration create high intensity beams of 10^{16} W/cm^2 to 10^{20} W/cm^2. The Titan laser at 1-ω (1054 nm) can deliver 150 J for 1 ps and 300 J for 40 ps. During our experiments we varied the laser energy between 30 J to 300 J with pulse durations between 0.5 ps to 40 ps.

We measured the laser spot size at low power using a microscope lens coupled to a CCD camera. This measurement method may be of limited accuracy because of B integral and main amplifier pump induced effects; however, they provide a qualitative measure of spot sizes as function of parabola focusing. Fig 3a shows the beam images displayed in log scale. Since most of our experiments are performed either at the best focus or 300 μm further upstream towards the focusing parabola, we characterized the laser beam spots at these locations. Without adaptive optics, the laser spot has multiple lobes when it is defocused. Assuming the brightest pixel is the center of the laser spot, the pixel intensity as a function of distance is plotted in Fig 3b, and Fig 3c which shows the cumulative laser energy fraction. We observe that the 50 % of the laser energy is contained within a 14 μm radius at the best focus and a 54 μm radius when defocused. In both cases, the entire laser energy is completely contained within our typical foil size of 300 μm x 300 μm. We use the defocused setting for many of our experiments in order to reduce Bremsstrahlung background that increases as the laser intensity increases while optimizing K-α yield which is measured to be fairly independent of laser intensity between 10^{17} W/cm^2 to 10^{19} W/cm^2 range[11]. A schematic of the Titan experiment is given in Fig 4. The micro-flag or micro-wire radiography targets were placed at the focal spot and rotated precisely to give an edge-on view to the imaging detectors at 2 locations.

III. Detectors

For high energy x-ray imaging, we use point projection onto either image plates and or a Gd_2O_2S scintillator backed by a Roper Scientific CCD camera. In this set-up, the angle between the incident backlighter laser and the detector was 16 degrees for the Gd_2O_2S/CCD detector and 40.7 degrees for the image plate detector.

Image Plate Detector: Image plates detect incoming x-ray photons on a uniform layer of small grain BaFBrI:Eu^{2+} crystals[14]. Excited electrons are trapped by empty halogen ion sites in the crystal, making metastable color centers capable of emitting radiation. Irradiation by a laser beam absorbed by the color centers excites the electrons again which quickly recombine with holes, and the recombination energy is transferred to the Eu ions, resulting in photo stimulated luminescence (PSL). For our experiment we use the BAS-SR type image plates manufactured by Fujifilm*.

Gd_2O_2S/CCD Detector: The other detector was a terbium-doped gadolinium oxysulfide (Gd_2O_2S:Tb) phosphor screen coupled to a front-illuminated CCD via a 1:1 fiber optic face plate. The phosphor converts incoming x rays into ~550 nm optical photons that are collected by the CCD detector. The CCD has 2084 pixels x 2084 pixels each 24 μm x 24 μm. This camera is manufactured by Roper Scientific Inc.

Single photon counting camera: In addition to the detectors used in point projection imaging, we also used two different types of spectrometers. The first was a single photon counting camera. This is a CCD camera that absorbs the x-ray photons directly in the silicon depletion region. When an x-ray photon is fully absorbed within a pixel, photoelectrons are created. For a silicon CCD, the pair creation energy is 3.65 eV at room temperature; a 1 keV x-

* "Certain commercial equipment, instruments, or materials are identified in this paper in order to specify the experimental procedure adequately. Such identification is not intended to imply recommendation or endorsement by the US government, nor is it intended to imply that the materials or equipment identified are necessarily the best available for the purpose."

ray photon, if absorbed completely in one pixel, will produce 274 photoelectrons. The number of photoelectrons collected on a pixel, then, is proportional to the incoming x-ray energy. Because of the fairly thin (16 μm) depletion layer of readily available CCDs, this detector is sensitive only up to x-ray energies of ~30 keV.

Quartz crystal spectrometer: The second spectrometer employed a transmission crystal in Laué geometry. This instrument uses a Qz(10-11) crystal curved to a radius of 254 mm[15]. The curvature of the quartz crystal focuses photons that are registered on an image plate located 254 mm behind the crystal. With this spectrometer we were able to record spectra up to 80 keV with a spectral resolution of 150.

IV. Laser Target

For radiography diagnostic development, we made micro-foil and micro-wire targets mounted on top of low-Z substrates to create small point sources for 1-dimensional and 2-dimensional radiography. Fig 5 shows an example of a Au micro-foil and a Au micro-wire target. These targets were fabricated by General Atomics. The micro-foil is a simple 300 μm x 300 μm x 5 μm Au foil held by a 6 μm diameter carbon fiber. The edge of this foil is cleanly sheared so that very little slag is seen from the edge-on view. Similar targets, made of Mo, Ag and Sm have also been tested in our experiments.

The micro-wire target was difficult to fabricate. The K-α radiator material (here, Au) was deposited on top of the approximately 4 μm to 5 μm thin CH substrate; then micro-machined into a small wire-like volume. We chose CH as the substrate in order to reduce the Bremsstrahlung background that scales as $\sim Z^2$. We chose the micro-machining process (instead of gluing a wire onto the substrate) so that the micro-wire had better contact with the substrate.

The short pulse laser hits the micro-wire side on. The laser spot sizes are bigger (as discussed in Section II) than the micro-wire size; the laser energy that misses the wire is intercepted by the substrate. The substrate plays the role of generating more refluxing hot electrons that may impact the fluor material, generating more K-α x rays.

V. RADIOGRAPHY RESULTS

V.1. 22 keV 2-D radiography with a micro-wire targets

In order to demonstrate 2-D radiography, we fabricated a test pattern consisting of an orthogonal stack of 1-dimensional slits (10 μm, 20 μm, 30 μm, 40 μm, 80 μm) on a 25 μm thick Au substrate. This test pattern was fabricated by a mask projection technique using an Excimer laser[16].

Using this pattern, we tested the performance of a 2-D radiography Ag micro-wire target that produces 22 keV x-rays containing both K-α and the Bremsstrahlung x-rays in this energy band. The expected source spectrum is quasi monochromatic as the source is filtered by the K-edge of the Ag filter. The laser energy for this shot was 242 J with a 40 ps pulse duration. We defocused the laser to have 50 % of laser energy contained within a 54 μm radius area. The resulting radiograph is shown in Fig 6. The diagonal sections with 10 μm, 20 μm and 30 μm grids are denoted in the figure. (For example, by a 10 μm grid, we mean that the wire widths are 10 μm, and the period or distance between adjacent wires is 20 μm.) With a 10 μm source size, we expected to resolve no better than 10 μm features as seen in this image. This image is taken with the Gd_2O_2S/CCD detector with an imaging magnification of 17.

We further analyzed this image to obtain the point spread function. We first created an ideal grid image by differentiating in the vertical and horizontal directions the image of a small, 30 μm

grid section. This ideal grid image was smeared by a 2D Gaussian resolution function, R(r) = exp[-($r^2/2\sigma^2$], and σ was varied until the smeared ideal grid most closely resembled the experimental image, as shown in Fig 7a. Fig 7b shows the horizontal and vertical line-outs from the central section of the experimental image *vs*. the best fit convoluted grid image. They match well implying that the fitted image reproduces the data quantitatively. The resulting fit gave σ = 4.2 μm, corresponding to a FWHM resolution of $2(2\ln 2)^{1/2}\sigma$ = 9.9 μm. This is consistent with the micro-wire size of 10 μm and proves that the high energy x-ray photons come mainly from the micro-wire bulk region and that the spatial resolution is limited by the micro-wire size. The Fourier transform of the resolution function gives the modulation transfer function (MTF), the result of which is:

$$M(k) = e^{-(k\sigma)^2/2}, \quad where \quad k = \frac{2\pi}{\lambda}$$

Here M(k) is the MTF, σ is the above fit point spread function parameter, λ is the period of the modulation. The resulting M(k) is plotted in Fig 7c. From this plot we deduce that we can achieve a 40 % MTF for 20 μm spatial features. This experiment was conducted with a laser energy of ~250 J. The MTF is expected to be higher with a higher energy laser, due to the higher signal in the experimental images.

V.2. 68 keV 1-dimensional and 2-dimensional radiography spatial resolutions with micro-foils and micro-wire targets

We have also tested Au Kα backlighter targets for 68 keV radiography in the micro-foil and micro-wire geometries. For 68 keV radiography, the Au grid test pattern (25 μm thick Au

substrate) used to test radiography at 22 keV, was inadequate as the attenuation length of Au at 68 keV is 163 μm. Instead, we measured the resolution using 1 mm thick Au plates that had several channels carved all the way through by EDM (Electrical Discharge Machining.) The edges of the channels served as knife-edge targets for testing the resolution and the EDM process minimized any slag that could be seen when viewed edge-on (Fig 8).

Two radiographs from these experiments are shown in Fig 9. The laser parameters used for these shots were similar to the settings used for the 22 keV Ag radiography described above. Fuji BAS-SR type image plates were used to record these images. The image in Fig 9a was taken with a 1-dimensional micro-flag target positioned in the vertical plane, perpendicular to the image. The 1-dimensional nature of the spatial resolution is clear; the spatial resolution is good only in the horizontal direction and only near the center of the image where the image plate sees only the edge of the Au test target because of its thickness. The image in Fig 9b was taken with a micro-wire target pointed at the image plate. Unlike the micro-foil target this image shows good spatial resolution in all directions. To quantify the spatial resolution, we fit line-outs across the edges (Fig 9b) to an edge spread function (ESF). The ESF is the integral response function of a Gaussian point spread function (PSF) which fits our knife-edge data well when combined with a linear background term:

$$ESF = I_0 \cdot erf\left(\frac{x}{\sigma}\right) + a_0 + a_1 x$$

where,

$$erf\left(\frac{x}{\sigma}\right) = \frac{2}{\pi}\int_0^{x/\sigma} e^{-t^2} dt$$

$$I_0, \sigma, a_0, a_1 = \text{fitting coefficients}$$

The fit results are shown as red lines in Fig 9 c and d. From this fit, we find the FWHM of the PSF to be 10.7 ± 1.0 μm in the 1-dimensional image and 12.3 ± 1.2 μm in the 2-D image, respectively. These measured numbers are larger than the actual foil thickness of 5 μm and wire size of 10 μm. This is likely caused by alignment errors of the thick test pattern target. After taking our 0.5 degree alignment accuracy into account, the resulting FWHM is consistent with the physical thickness of the micro-foil.

In this direct comparison of micro-foil and micro-wire radiography, it is clear that the K-α emission is confined to the bulk fluor material and any plasma blow-off or substrate emission does little to degrade the spatial resolution.

V.3 Radiometric intensities of micro-flag and micro-wire sources

The differences in relative photon output between the micro-flag and micro-wire targets were apparent in these experiments. The images are presented in PSL units which linearize the image plate scanner output digital scale. We denote the signal levels in the line-outs by I_{sig}_1D and I_{sig}_2D and the background levels by I_{bkg}_1D and I_{bkg}_2D. We measure I_{sig}_1D=1.08 ± 0.03, I_{bkg}_1D=0.21 ± 0.15, I_{sig}_2D=0.25 ± 0.018 and I_{bkg}_2D=0.088 ± 0.011. From these numbers we deduce that the number of x-ray photons emitted by the source and captured by the image plates is 4 times higher for the 1-dimensional micro-flag targets than for the 2-dimensionoal micro-wire targets.

The radiography signal level difference (I_{sig}_1D vs I_{sig}_2D) may be explained by the size of the area on the fluor intersected by the laser. For the micro-flag target, 100 % of the laser energy struck the Au material whereas for the micro-wire only 25 % of the laser energy struck the Au as

we operated the laser in 'defocused' mode for these shots. As discussed in section II, the defocused laser spot has a radius of 54 μm. If the laser spot is Gaussian, the intersection with a 10 μm diameter wire is only 25 % of the total beam area.

However, we observe that the radiometric difference in the signal level between the 1-dimensional micro-flag targets and the 2-dimensional micro-wire targets is not the same as the difference determined by measurements of only the K-α yield. In Fig 10, we compare micro-flag and micro-wire target K-α spectra measured by the single photon counting camera. The micro-flag target was a 100 μm x 100 μm x 5 μm Mo foil and the micro-wire target was a 150 μm x 20 μm x 10 μm Mo wire on a 150 μm x 150 μm x 10 μm Al substrate. The laser energy was 280 J and we used the best focus (σ = 6.2 μm) to irradiate the micro-wire. After correcting for the filters and shot-to-shot differences in the laser energy, our measurements indicate that the number of hits in the K-α peak for the micro-wire target is 10 times less than the number from the micro-flag targets with an error of 30%. The factor of 10 differences in K-α yields cannot be accounted for by the mass difference nor the difference in the size of the area struck by the laser. The volume of Mo in the micro-wire target is 30000 μm^3, and the volume of Mo in the micro-flag target is 50000 μm^3, so the two targets have similar mass. Furthermore, the micro-wire target accepts 90 % of the focused laser energy.

One reason why the 1-dimensional radiography signal is much higher than the K-α only signal is that, in a radiography imaging experiment, the signal is a combination of both K-α and Bremsstrahlung photons within the quasi-monochromatic filtering window. This gives enhances the photon signals for radiography.

VI. K-α conversion efficiencies for micro-foil targets

We have determined K-α conversion efficiencies as function of target material up to the Pb K-α line of 75 keV. In these measurements the targets were 0.5 mm x 4 mm x 25 μm thick in size. The laser parameters were 40 ps at 220 J with a focal spot of ~54 μm in diameter yielding a laser intensity of 2×10^{17} W/cm^2.

For this experiment, we measured the efficiency of converting laser energy to K-α x-rays using two different spectrometers: the single photon counting (SPC) CCD camera for K-α energies between 10 keV and 30 keV, and the quartz crystal spectrometer for K-α energies between 15 keV and 78 keV. Details of these detectors were given in section II. Fig 11a shows an example of the spectrum from a Ag micro-wire target measured by the SPC detector. The K-α and K-β peaks are clearly visible. We count the number of hits above the background in the K-α and K-β peaks and multiply by the photon energy to obtain $E_{K\text{-}\alpha}(measured)$, the measured amount of K-α or K-β radiation in the detector . The conversion efficiency is, then, calculated by:

$$\varepsilon_{conv} = (E_{K\text{-}\alpha}(measured) \cdot 4\pi)/(\varepsilon_{detector} \cdot \varepsilon_{single\_hit} \cdot T_{filter} \cdot \Omega_{detector})/E_{laser}$$

where ε_{conv} is the conversion efficiency, $\varepsilon_{detector}$ is detector quantum efficiency ε_{single_hit} is the probability that all of the 22 keV energy from a single photon is captured in one pixel, T_{filter} is the transmission factor through the filter materials, and $\Omega_{detector}$ is the detector solid angle. The detection efficiency for the SPC is absolutely calibrated using a Cd109 radioactive source[17]. The calibration allows us to determine the combined efficiency $\varepsilon_{detector}$ x $\varepsilon_{single_hit.}$to be (6.24 ± 0.93) % for Fe 55 (1.47 ± 0.22) % for Cu K-α and (0.134 ± 0.02) % for Ag K-α. Knowing these efficiencies allows us to measure the absolute conversion efficiencies for Cu, Mo, Ag, and Sn

targets with this detector. Details on this single photon counting camera efficiencies will be published[18].

For the higher Z target materials we used the crystal spectrometer as described in Ref 19. Fig 11b shows data for Sn, Sm, Ta, Au and Pb target materials. Again we count the number of hits above the background. The detector (image plate) response is calculated assuming that the BaFBrI:Eu^{2+} phosphor material is 121 μm thick with a density of 3.07 g/cm^3, then using the standard energy dependent x-ray absorption coefficients for this material. The Qz crystal response is calculated using the XOP simulation code for a Laue geometry[20]. This procedure gives only a relative response function for the crystal spectrometer. Since both the crystal spectrometer and the SPC can measure Ag K-α photons, the relative responses of the crystal spectrometer were scaled so that the measurement of the Ag K-α made by the two instruments agreed. This provided an absolute calibration of the crystal spectrometer for the other measurements. The resulting conversion efficiencies divided by the ratio of the material density to the Ag density are plotted in Fig 12. The errors (35%) on these measurements are from the statistical error of the K-α peak counts, the error on the single photon counting camera detection efficiency (15%) , the error on the detector efficiency (20%,) and the uncertainty in the crystal spectrometer efficiency (20%).

While there are a few analytical model of femtosecond K-a x-ray generations[21], we compare these results with Monte Carlo (MC) simulations using the ITS (Integrated Tiger Series) code[22]. The MC simulation of K-α x-ray production proceeds in two steps. First, a hot electron temperature is determined from the formula[23]:

$$T_{hot} = \left(\frac{I \cdot \lambda^2}{10^{19} \frac{W}{cm^2} \cdot \mu m^2} \right)^{1/3} \cdot MeV$$

where $\boldsymbol{I}$ is the laser intensity in W/cm^2 and $\boldsymbol{\lambda}$ is the laser wavelength in μm. Electrons are generated having energies taken from the Boltzman distribution characteristic energy. Each electron is then transported through the target material using the ITS Monte Carlo code. In the calculation, the electrons are injected at the surface of the solid target into a cone of half-angle 26º into the target. The ITS simulation determines the number of K-α x-ray photons per hot electron per steradian as a function of angle. The number of hot electrons as a function of laser intensity is determined by the formula:

$$\varepsilon_{hotelectrons} = 0.096 \cdot \left(\frac{I}{10^{18} \frac{W}{cm^2}} \right)^{0.29}$$

where $\boldsymbol{I}$ is the laser intensity in W/cm^2. This equation is derived from experimental measurements by Yasuike et al[24]. By multiplying the yield of K-β photons per electron per steradian from the first step by the number of hot electrons from the second step, we obtain the K-α yield per steradian.

The resulting output of the MC simulations is noted as the red line in Fig 12. The current simulation set doesn't account for electron refluxing[25] which can increase K-α production. Note that we have normalized the simulated conversion efficiencies so that it agrees with the measured Ag K-α data by multiplying each point on the curve by a constant correction factor of 2. This correction factor may be accounted for by electron refluxing in our target.

VII. CONCLUSION

We have obtained high-resolution, high-energy radiographs using a high-intensity laser focused onto micro-flag and micro-wire targets. We find that the high-energy K-α photon emission is confined to the target volume resulting in a spatial resolution in the images defined

by the fluor material size. When viewed edge-on and using 5 μm to 10 μm micro-wire and micro-flag targets, we obtained spatial resolutions of ~10 μm FWHM. We find that the K-conversion efficiencies for the micro-wire targets are a factor of 10 lower than for the micro-flag targets. However, in practical radiography experiments, some fraction of the non-K-α Bremsstrahulung photons having energies around the K-α energy contribute to the number of photons collected increasing the signal level by a factor of 2. Finally, we measured K-α conversion efficiencies up to the 75 keV Pb K-α line; the results are compared to the Monte Carlo (ITS) simulations with reasonable agreement. At 75 keV, the K-α conversion efficiency, 2.5×10^{-5}, is 4 times lower than the conversion efficiency at the 22 keV Ag K-α line.

REFERENCES

[1]E. Andersson, G. Holzer and E. Forster, Journal of Applied Physcis, **90**, 6, 3048 (2001).

[2]R. Toth, S. Foumaux, T. Ozaki, M. Servol, and J. C. Keiffer, Phys. Of Plasmas 14, 053506 (2006).

[3] L.J. Waxer, D.N. Maywar, J.H. Kelly *et al*., Optics & Photonics News **16**, 30 (2005).

[4]D.H. McDaniel, M.G. Mazarakis, D.E. Bliss *et al*., Proceedings of the Fifth International Conference on Dense Z-Pinches, Albuquerque, 2002, edited by J. Davis, C. Deeney, and N.R. Pereira (AIP, Melville, NY, 2002), p.23.

[5] J.A. Paisner, E.M. Campbell, and W.J. Hogan, Fusion Technology **26**, 755 (1994).

[6] B.A. Remington, G. Bazan, J. Belrak *et al*., Metall. Mater. Trans. A **35A**, 2587 (2004); B.A. Remington et al., Mat. Sci. Tech. 22, 474 (2006).

[7] T.R. Dittrich, S.W. Haan, M.M. Marinak *et al*., Phys Plasmas **6**, No. 5, 2164 (1999).

[8] J. Edwards et al., PRL 92, 075002 (2004).

[9]K.T. Lorenz, M.J. Edwards, S.G. Glendinning, A.F. Jankowski, J.McNaney, M.Pollaine, and B.A. Remington, Phys. Plasmas **12**, 056309 (2005)

[10] M.H. Key, M.D. Cable, T.E. Cowan *et al*., Phys Plasmas **5**, 1966 (1998).

[11]H. S. Park *et al.*, Phys Plasmas **13**, 056309 (2006).

[12] A. Benuzzi-Mounaix et al., Plasma Phys. Control. Fusion, **48**, B347, (2006).

[13] D. Strickland and G. Mourou, Opt. Commun., **56** 219-221 (1985).

[14] M. Sonoda, M. Takano, J. Miyahara and H. Kato, Radiology, **148**, 833 (1983).

[15] J. Seely et al., High Energy Density Physics 3, 263 (2007).

[16] Glenn Ogura and Ruediger Hack, Medical Device & Diagnostic Industry, March (2006).

[17] H. S. Park et al., Proceedings of SPIE, **5196**, 213 (2004).

[18] B. Maddox, H. S. Park et al., RSI paper, in preparation (2008)

[19] R. Tommasini et al., , in *15th International Conference on Atomic Processes in Plasmas*, edited by J. D. Gillaspy, J. J. Curry, and W. Wiese, AIP Conference Proceedings 926, Melville, New York: American Institute of Physics, 2007, pp. 248 - 255.

[20] M. Sanchez del Reio and R.J. Dejus, Proceedings of SPIE **3152**, 148 (1997).

[21]D. Salzmann, Ch. Reich, I. Uschmann, and E. Forster, Phys. Review. E. **65**, 036402 (2002).

[22] J. A. Halbleib, R. P. Kensek, G. D. Valdez, IEEE Trans on Nuc. Sci. **39**, No. 4, 1025 (1992).

[23] F.N. Beg et al., Phys Plasmas 4, 457 (1997).

[24] K. Yasuike, M.H. Key, S.P. Hatchett, R.A. Snavely, and K.B. Wharton, Rev. Sci. Instrum **72**, 1236 (2001).

[25]J. Myatt et al., Phys Plasmas **14**, 056301 (2007).

This work performed under the auspices of the U.S. Department of Energy by Lawrence Livermore National Laboratory under Contract DE-AC52-07NA27344.

Figure Captions

Fig 1. Examples of high-energy-density experiments that require high energy backlighters on NIF. The left panel is a configuration for a material strength experiment where the ripple growth factors are measured via face-on radiography. (b) The right panel is the mid to high-Z capsule implosion experiments where capsule implosion symmetry will be studied. All require > 40 keV radiography due to the high areal density thickness of the samples.

Fig 2. Sketch of point projection radiography using ~5 μm thin 1-dimensional micro-foil sources and ~10 μm x 10 μm x 300 μm wire micro-wire source for 2-D radiography. For high energy K-α radiography, the x-ray radiation is confined within the fluor target material. The small size of the targets produces radiographs with high spatial resolution.

Fig 3. Laser spot image at its best focus and in a defocused condition where the target is placed300 μm towards the parabola. 50 % of the laser energy is contained within a 14 μm radius at the best focus and within a 54 μm radius for the defocused case.

Fig 4. Titan experimental set-up. Two different types of imaging devices (Image Plate and Gd_2O_2S/CCD imager) and two different spectrometers (single photon counting camera and curved Qz crystal spectrometer) were employed to measure spatial resolution and K-α conversion efficiencies.

Fig 5. Fabricated micro-foil and micro-wire targets. These are examples used for Au K-α radiography. We have tested Mo, Ag and Sm targets that are fabricated with similar geometries. The radiographs are taken along an axis providing an edge-on view of the micro-wire or micro dot.

Fig 6. The results of Ag K-α radiography with micro-wire target. The diagonal sections with 10 μm, 20 μm and 30 μm grids are denoted. The central 10 μm grid region is well resolved.

Fig 7. MTF analysis of the radiographs in Fig 5. The point spread function is obtained by finding the best match of the data with an ideal grid image convoluted with the point spread function. We obtain a ~40 % MTF for 20 μm periods with the 250 J Titan laser. , Improved MTFs are expected with higher energy lasers.

Fig. 8. Test target for Au radiography (68 keV). The target is made of 1 mm thick Au material with edges machined using EDM.

Fig 9. Radiography results from the Au micro-flag and micro-wire targets. The 1-dimensional and 2-dimensional nature of the images are clear. The edges were fit to an edge spread function (see text.).

Fig 10. Difference in K-α yield between micro-flag and micro-wire targets measured by the single photon counting camera. The histograms are background subtracted. After accounting for

the difference in laser energy and filter settings, the difference in the K-α yield between these two types of targets is a factor of 10.

Fig 11. K-α yield measurements using the single photon counting camera (a) and the curved Qz crystal spectrometer (b) for various target materials. We measure absolute K-α conversion efficiencies using the single photon counting camera at 8 keV to 25 keV and relative conversion efficiencies using Qz spectrometer at 20 keV to 80 keV. By normalizing the K-efficiencies at 22 keV, we measure the absolute K-α efficiencies from 17 keV to 75 keV.

Fig 12. The K-α conversion efficiency of different target materials. The ITS Monte Carlo simulation is plotted.

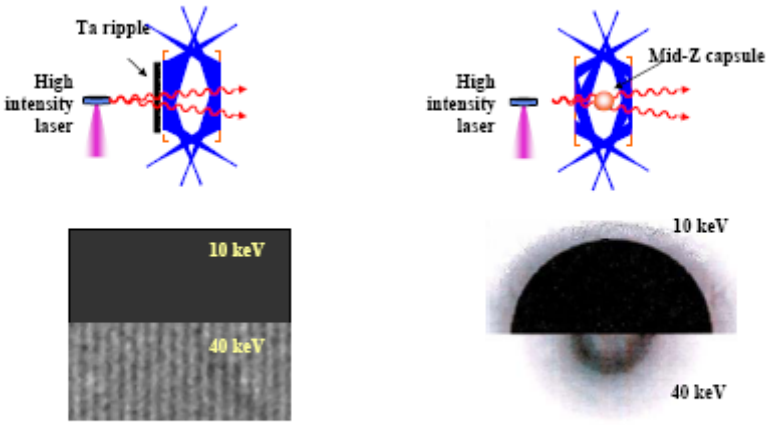
Ta ripple
High intensity laser
10 keV
40 keV
Mid-Z capsule
High intensity laser
10 keV
40 keV

Fig1

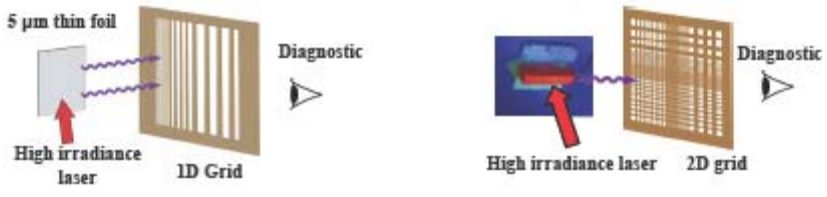
5 μm thin foil
Diagnostic
High irradiance laser
1D Grid
Diagnostic
High irradiance laser
2D grid

Fig 2

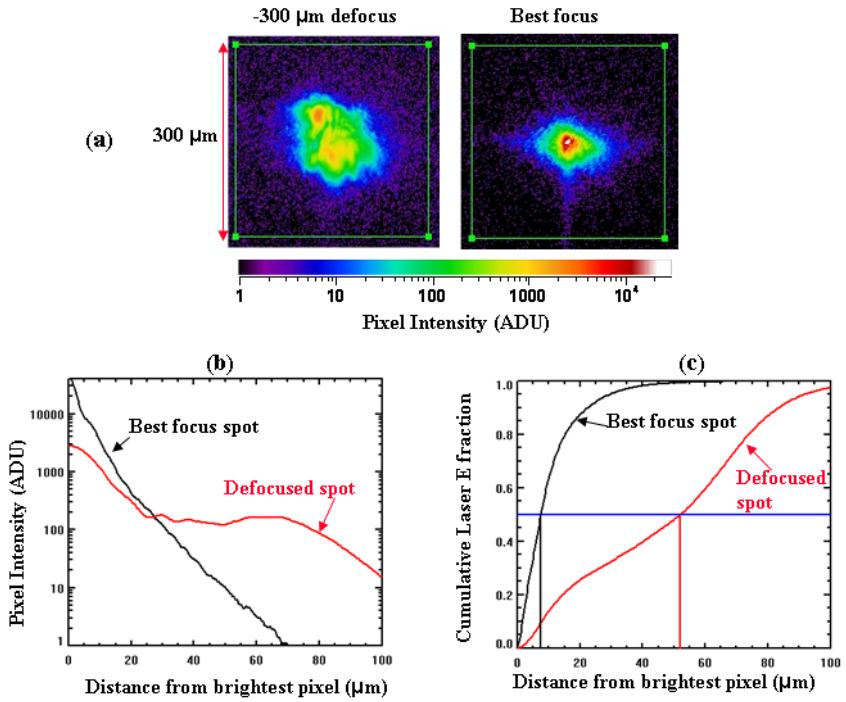
-300 µm defocus
Best focus
(a)
300 µm
1
10
100
1000
10⁴
Pixel Intensity (ADU)
(b)
Best focus spot
Defocused spot
Pixel Intensity (ADU)
Distance from brightest pixel (µm)
(c)
Best focus spot
Defocused spot
Cumulative Laser E fraction
Distance from brightest pixel (µm)

Fig 3

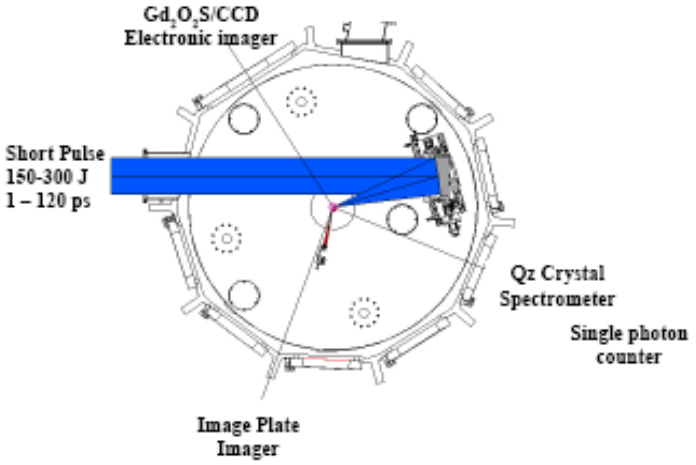
Gd2O2S/CCD
Electronic imager
Short Pulse
150-300 J
1 – 120 ps
Qz Crystal
Spectrometer
Single photon
counter
Image Plate
Imager

Fig 4

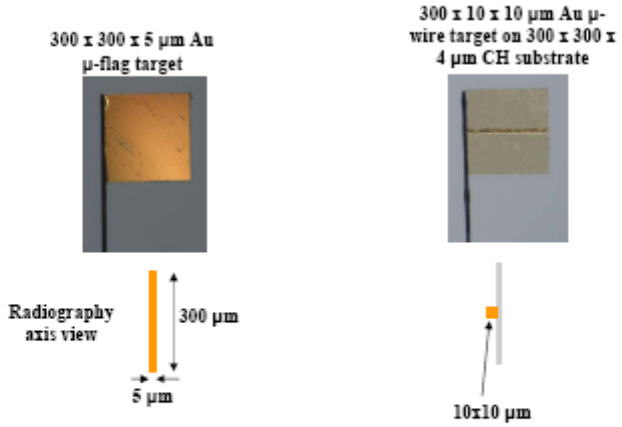
300 x 300 x 5 μm Au
μ-flag target
300 x 10 x 10 μm Au μ-
wire target on 300 x 300 x
4 μm CH substrate
Radiography
axis view
300 μm
5 μm
10x10 μm

Fig 5

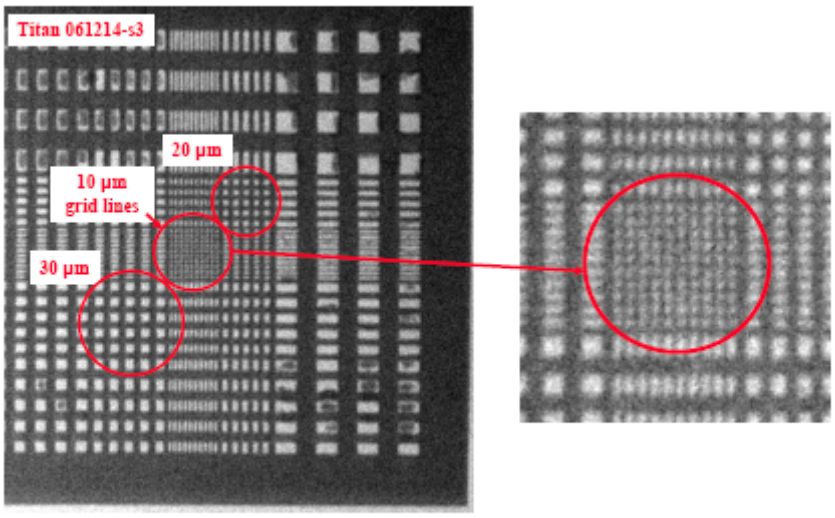
Titan 061214-s3
20 μm
10 μm
grid lines
30 μm

Fig 6

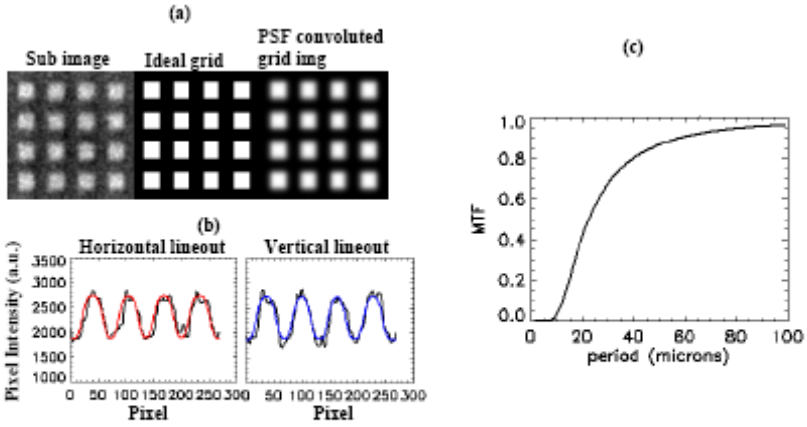
(a)
Sub image
Ideal grid
PSF convoluted grid img
(b)
Horizontal lineout
Vertical lineout
Pixel Intensity (a.u.)
3500
3000
2500
2000
1500
1000
0 50 100 150 200 250 300
Pixel
50 100 150 200 250 300
Pixel
(c)
MTF
1.0
0.8
0.6
0.4
0.2
0.0
0 20 40 60 80 100
period (microns)

Fig 7

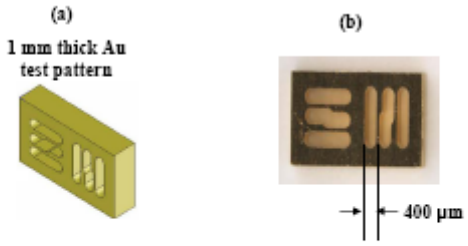
(a)
1 mm thick Au
test pattern
(b)
400 µm

Fig 8

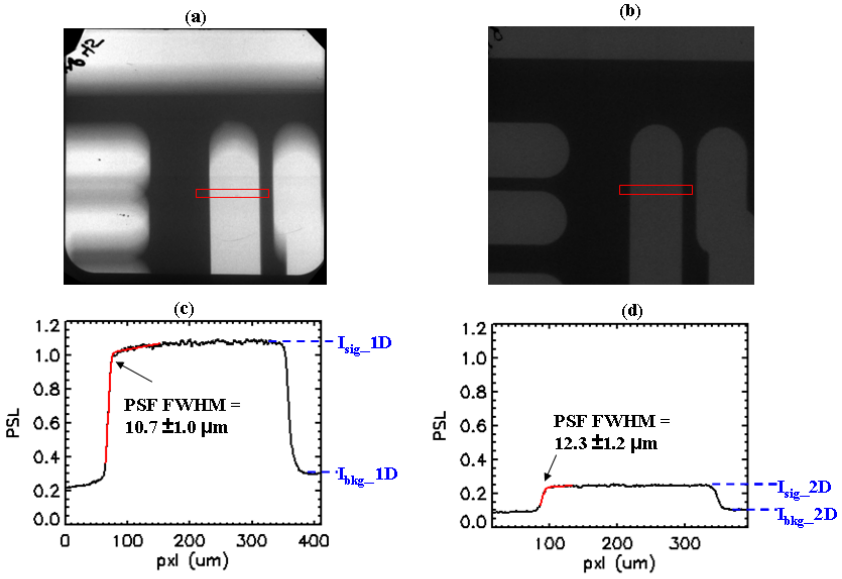
(a)
(b)
(c)
(d)
PSF FWHM =
10.7 ±1.0 μm
PSF FWHM =
12.3 ±1.2 μm
PSL
pxl (um)
I_{sig_1D}
I_{bkg_1D}
I_{sig_2D}
I_{bkg_2D}

Fig 9

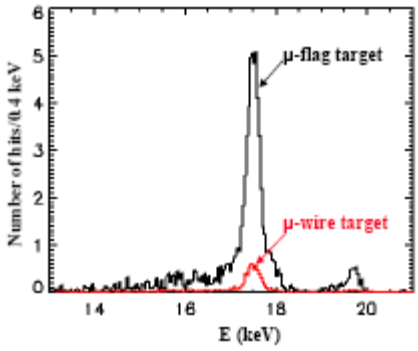
μ-flag target
μ-wire target
Number of hits/0.4 keV
E (keV)

Fig 10

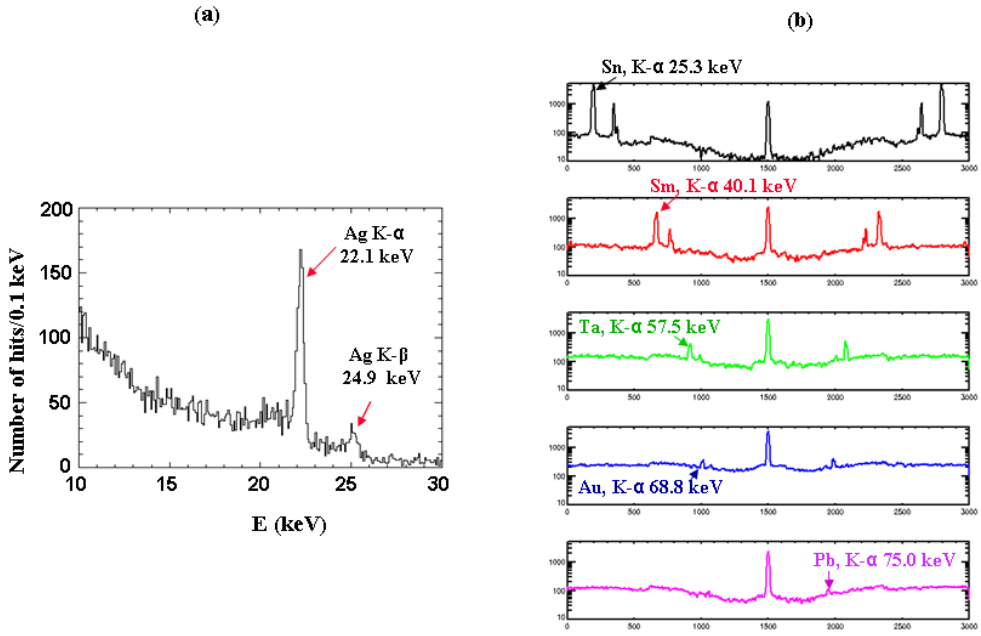
(a)
(b)
Number of hits/0.1 keV
E (keV)
Ag K-α
22.1 keV
Ag K-β
24.9 keV
Sn, K-α 25.3 keV
Sm, K-α 40.1 keV
Ta, K-α 57.5 keV
Au, K-α 68.8 keV
Pb, K-α 75.0 keV

Fig 11

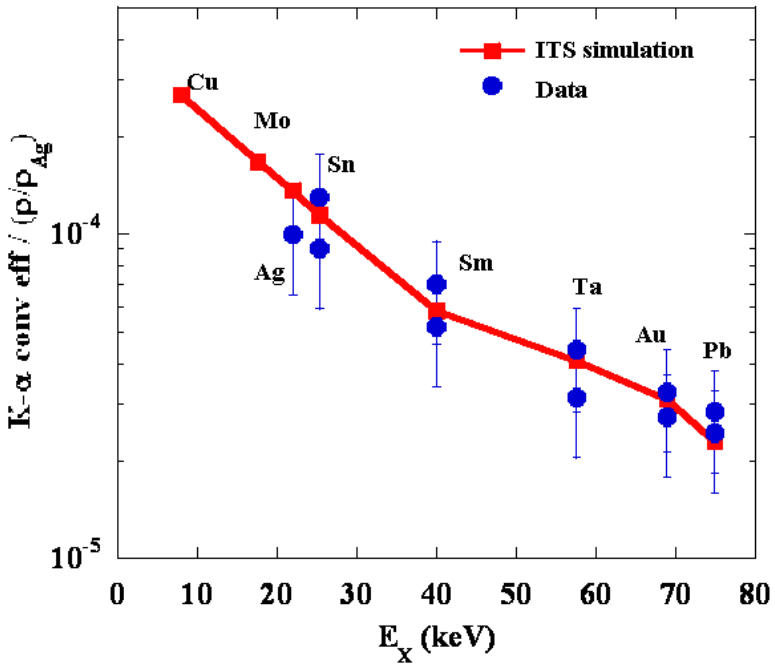
ITS simulation
Data
Cu
Mo
Sn
Ag
Sm
Ta
Au
Pb
K-α conv eff / (ρ/ρ_Ag)
E_X (keV)

Fig 12